Dual Null Detection Points Removal and Time-Domain Sensitivity Analysis of a Self-Injection-Locked Radar for Small-Amplitude Motion Sensing

Dongyang Tang, *Student Member, IEEE*, Davi V. Q. Rodrigues, *Graduate Student Member, IEEE*, Michael C. Brown, *Graduate Student Member, IEEE*, and Changzhi Li, *Senior Member, IEEE*

***Abstract*— Compared with a conventional Doppler radar in which target displacement results in phase modulation, target displacement in a self-injection-locked oscillator (SILO)-based radar results in frequency modulation. Since the instantaneous phase is the time integral of frequency, the SILO-based radar is considered to have higher sensitivity than the conventional Doppler radar. However, a direct comparison between the SILO-based radar and the conventional Doppler radar is still needed to quantitatively understand the sensitivity difference. This article provides a rigorous time-domain analysis of the sensitivity of the SILO-based radar with a delay-based frequency demodulator for small-amplitude periodic motions. The analysis follows an approach similar to the time-domain analysis for the conventional Doppler radar. It reveals that two null detection point mechanisms could arise in SILO-based radar systems. The target distance may introduce one null detection point, and the delay added in the frequency demodulator may introduce another. Furthermore, this article also proposes an SILO-based radar with dual null detection points' removal. Unlike the Doppler radar, where I/Q demodulation eliminates the null detection point introduced by the target distance, I/Q demodulation in the SILO-based radar only eliminates the null detection point introduced by the delay cable. To overcome the other null detection point mechanism, a phase shifter is introduced after the LNA. Experiments were carried out to validate the proposed time-domain analysis and demonstrate that both the techniques need to be used simultaneously to remove both null detection points in the system. The sensitivity comparison was performed using a conventional Doppler radar and an SILO-based radar built with identical microwave components.**

***Index Terms*— Doppler radar, injection-locking, linearity, microwave motion sensors, null detection point, self-injection-locked oscillator (SILO) radar, sensitivity.**

I. INTRODUCTION

MICROWAVE low-cost radars have shown great potential for noncontact motion detection. Since radar sensors offer accurate measurements under noncontact operation, they may play a crucial role in several areas, including disaster rescue [1]–[3], gesture recognition [4], [5], fall detection [6]–[8], structural health monitoring [9]–[11], and vital sign monitoring [12]–[20]. Radar-based structural health monitoring relies on the assessment of the structural proprieties by remotely detecting the reciprocal motion of a structure. Similarly, radar-based vital-sign sensing detects the periodic motion of the chest wall caused by the cardiopulmonary phenomena or breathing. These remote sensing techniques, along with the rapid development of the Internet of Things (IoT), big data science, and artificial intelligence, could significantly improve the quality of service provided by the healthcare system, infrastructure maintenance, and consumer products sector.

Over the past decade, the self-injection-locked oscillator (SILO)-based radar has attracted researchers' attention due to its simple architecture and high sensitivity, especially for vital sign sensing [20]–[23]. Since it does not require a local oscillator (LO), the SILO-based radar also provides inherent clutter rejection, particularly to stationary clutters, which are common sources of interference in the conventional Doppler radar [13]. Moreover, the simplest SILO-based radar requires only an injection-locked oscillator as the active radio frequency (RF) component due to its high sensitivity [22], as shown in Fig. 1(a).

While the time-varying position of targets generates phase modulation in the transmitted signal for a conventional Doppler radar, the target displacement induces frequency modulation in the transmitted signal for an SILO-based radar [14], [20]. Because the phase is the time integral of the frequency, the SILO-based radar inherently integrates and amplifies the targets' Doppler motion in the phase domain. In [13] and [22], the SILO-based radar's operation was studied using frequency-domain analysis. However, the conventional analysis for the Doppler radar follows a time-domain approach [15], making it challenging to provide a quantitative sensitivity comparison between the two radar architectures.

Manuscript received 6 May 2022; accepted 6 June 2022. This work was supported by the National Science Foundation (NSF) under Grant ECCS-2030094 and Grant ECCS-1808613. *(Corresponding author: Dongyang Tang.)*

The authors are with the Department of Electrical and Computer Engineering, Texas Tech University, Lubbock, TX 79409 USA (e-mail: dongyang.tang@ttu.edu; davi.rodrigues@ttu.edu; michael.c.brown@ttu.edu; changzhi.li@ttu.edu).

Color versions of one or more figures in this article are available at https://doi.org/10.1109/TMTT.2022.3186299.

Digital Object Identifier 10.1109/TMTT.2022.3186299

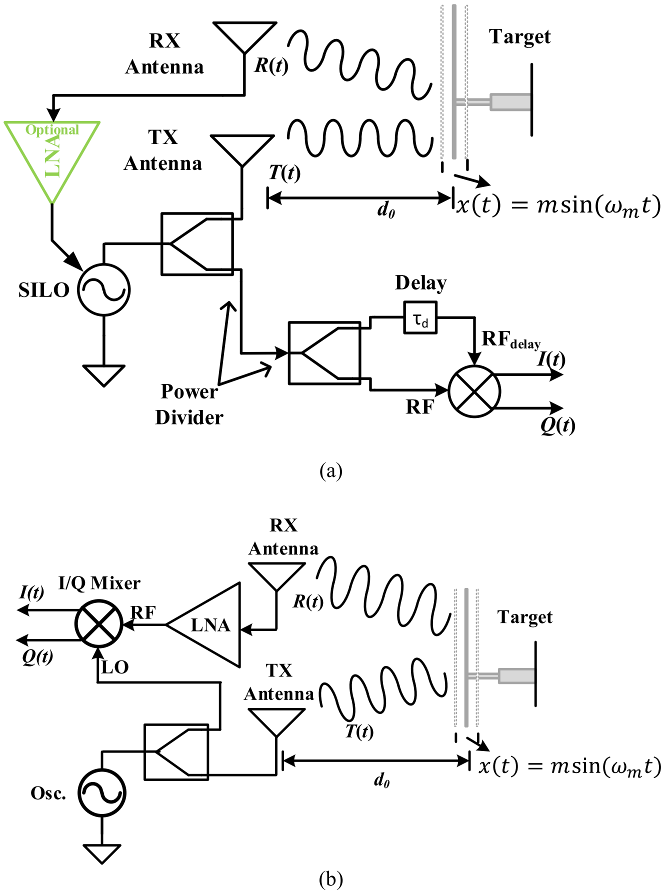

(a)

(b)

Fig. 1. Radar-based motion detection. Block diagram for (a) SILO radar and (b) Doppler radar.

In this article, a rigorous time-domain analysis for the sensitivity of the SILO-based radar for small-amplitude periodic motion is derived. It follows the identical time-domain-based methodology as that used for the conventional Doppler radar sensitivity analysis. Therefore, the sensitivity equations for both the SILO-based radar and the conventional Doppler radar have a similar format for easier comparison. The proposed analysis also reveals that the SILO-based radar with delay-based frequency demodulation has two different types of null detection points: one null detection point that is encountered at every quarter wavelength distance from the SILO-based radar to the target and another may be introduced by the delay added in the frequency demodulator. A null detection point is a condition that the baseband signal only has a DC component plus even-order harmonics, and the fundamental frequency of the target displacement cannot be recovered. The detail of the null detection point will be discussed in Section II. In contrast, the conventional Doppler radar has only one null detection point introduced by the distance between the target and the Doppler radar sensor. This can be overcome by adopting quadrature demodulation (using in-phase and quadrature I/Q channels) [14], [24]. In this article, the proposed time-domain analysis shows that when quadrature demodulation is adopted in the SILO-based radar, it cannot eliminate the null detection point introduced by the distance. Instead, it can be used to eliminate the null detection point introduced by the delay added in the frequency demodulator. One way to address the null detection point introduced by the target distance in an SILO-based radar is the path diversity transmission, which switches between two orthogonal paths [25]. However, it did not optimize for the sensitivity. In [26] and [27], the null detection point from the target distance of a Doppler radar was addressed with a phase shifter in the receiver path. According to our analysis, a similar approach should also work for an SILO-based radar to achieve the best sensitivity with a simple search algorithm. Therefore, an SILO-based radar that eliminates both null detection points simultaneously can be designed by combining the aforementioned techniques. It is worth noting that in [28] and [29], a phase shifter was also used in an SILO-based radar,but the function was different. In [28], the phase shifter was used to eliminate the large frequency shift caused by the strong clutter, which may cause the SIL mechanism to fail. In [29], the phase shift was adjusted repeatedly, switching between 0° and 90° to remove the output distortion due to the target's large displacement.

The rest of the article is organized as follows. Section II provides the theory and sensitivity analysis for the Doppler radar and the SILO-based radar using time-domain analysis. Section III explains the proposed architecture. To validate the analysis and demonstrate the proposed architecture's effectiveness for removing the dual null detection points, the experimental results are presented in Section IV. The sensitivities of the conventional Doppler and SILO-based radars are also compared. Finally, the conclusions are drawn in Section V.

II. THEORY AND SENSITIVITY ANALYSIS

A. Doppler Radar

The conventional Doppler radar architecture is shown in Fig. 1(b). A free-running oscillator generates a sinusoidal signal, and it is transmitted toward a target of interest through a transmitting (TX) antenna. The transmitted signal $T(t)$ can be written as

$$T(t) = \sin(2\pi f t) \tag{1}$$

where f is the frequency of the free-running oscillator. After being reflected by the target, the signal is picked up by a receiving (RX) antenna. The received signal $R(t)$ is the delayed and attenuated version of $T(t)$. For simplicity, and without loss of generality, the attenuation and constant phase shift are ignored in this analysis, and $R(t)$ is given by

$$R(t) = \sin(2\pi f(t - t_d(t))) \tag{2}$$

where $t_d(t)$ is the time delay between the transmitted and received signals. Although (1) and (2) have the same amplitude for simplicity of the equation, it needs to be noted that significant gain is required for the RF front-end to achieve this. Assuming the distance from the target to the radar is d_0 and the target moves periodically with an amplitude of m and a fundamental angular frequency of ω_m

$$t_d(t) = \frac{2d}{c} = \frac{2(d_0 + m\sin(\omega_m t))}{c} \tag{3}$$

where d is the total distance between the target and the radar, and c is the speed of light. The received signal is amplified by a low-noise amplifier (LNA) and then down-converted to in-phase and quadrature baseband signals $I(t)$ and $Q(t)$ by a quadrature mixer. The same oscillator output is sent to the mixer as the LO signal through a power divider. $I(t)$ and $Q(t)$ can be written as

$$I(t) = \frac{1}{2}\cos\left(\frac{4\pi m \sin(\omega_m t)}{\lambda} + \frac{4\pi d_0}{\lambda}\right) \tag{4}$$

$$Q(t) = \frac{1}{2}\sin\left(\frac{4\pi m \sin(\omega_m t)}{\lambda} + \frac{4\pi d_0}{\lambda}\right). \tag{5}$$

With low-pass filtering and applying a fast Fourier transform (FFT) on the baseband signal, the periodicity of the target movement ω_m can be extracted [30]. Since $\sin(x) \approx x$ and $\cos(x) \approx 1-(x^2/2)$ when x is small, if only one channel output is used, there is a chance that the output signal is $\cos(x)$ and that the FFT output only has the DC component and the second-order harmonic depending on the constant phase $4\pi d_0/\lambda$. For example, considering only $I(t)$ is used (6), as shown at the bottom of the next page. When the target distance satisfies the top equation, it is at the null detection point. When the target distance satisfies the bottom equation, it is at the optimal detection point. Hence, both $I(t)$ and $Q(t)$ are needed to recover the fundamental frequency with different target distances. $4\pi/\lambda$ in (6) is defined as modulation gain for the Doppler radar.

B. SILO-Based Radar

The injection-locked oscillator's output phase dynamics were derived by Adler [31] originally in 1946. Later, it was derived by different people with somewhat different approaches [32]–[36]. Adler's equation is given below

$$\frac{d\theta}{dt} = \omega_0 - \omega_{\text{inj}} - \omega_L \sin(\theta) \tag{7}$$

$$\omega_L = \frac{\omega_0 |I_{\text{inj}}|}{2Q|I_{\text{osc}}|} \tag{8}$$

where θ is the output signal phase referred to the injection signal, ω_0 is the angular frequency of the free-running oscillator, ω_{inj} is the angular frequency of the injection signal, ω_L is the angular frequency locking range, Q is the quality factor of the oscillator's LC tank, I_{inj} is the amplitude of the injection signal, and I_{osc} is the amplitude of the free-running oscillator output. In an SILO, the oscillator output is fed back to the injection port, so the phase difference θ between the output and injection signals is known. Under steady-state, the oscillator output is locked to the injection signal, and so the frequency of the oscillator ω_{out} can be calculated from (7) by setting $d\theta/dt$ to zero, as shown in the following:

$$\omega_{\text{out}} = \omega_{\text{inj}} = \omega_0 - \omega_L \sin(\theta). \tag{9}$$

The equation above indicates that the phase delay change provokes frequency changes in the output signal. Furthermore, the relationship between the phase and the frequency changes is not a linear function, and instead, it follows a sinusoidal function. For the SILO-based radar, the oscillator is always assumed to be locked when the target movement is slow, and $d\theta/dt$ being zero still holds. Also, θ is decided by the round trip time delay of the RF signal. From (3), it can be shown that

$$\theta = \frac{4\pi f d}{c}. \tag{10}$$

Substituting (10) into (9) and replacing ω with $2\pi f$

$$f_{\text{out}} = f_0 - f_L \sin\left(\frac{4\pi f_{\text{out}} d}{c}\right). \tag{11}$$

This equation is an implicit function and cannot be solved easily with a closed-form expression. It can be reformulated as

$$\Delta f = -f_L \sin\left(\frac{4\pi(f_0 + \Delta f)d}{c}\right) \tag{12}$$

where $\Delta f = f_{\text{out}} - f_0$. It should be noted that $f_L \ll f_0$ under small signal injection. Like in the Doppler radar analysis, the target distance

$$d = d_0 + d_m = d_0 + m\sin(\omega_m t) \tag{13}$$

where d_m represents the target displacement. Substituting (13) into (12)

$$\Delta f = -f_L \sin\left(\frac{4\pi(f_0 d + \Delta f d_0 + \Delta f d_m)}{c}\right). \tag{14}$$

For the right side of (14), $\Delta f \times d_m$ is small and can be ignored. If $\Delta f \times d_0$ can also be ignored, (14) can be approximated as

$$\Delta f \approx -f_L \sin\left(\frac{4\pi f_0 d}{c}\right). \tag{15}$$

As all the variables on the right side of (15) are known, f_{out} can be calculated directly

$$f_{\text{out}} \approx f_0 - f_L \sin\left(\frac{4\pi f_0 d}{c}\right). \tag{16}$$

This approximation can be justified by appreciating that the variable of interest is the target movement frequency instead of the actual distance. Therefore, as long as the error generated by this approximation has good linearity, the target movement frequency can still be detected with this approximation. To validate the approximation, (11) can be solved numerically and compared with the result using (16). Fig. 2 shows the simulation results from MATLAB. Fig. 2(a)–(d) shows the frequency versus distance. The x-axis is the distance d including the average distance plus the displacement in meters, and the y-axis is the frequency f_{out} in Hz. Each plot has two curves, where the solid curve is the numerical solver's result for (11), and the dashed curve is the result calculated from (16). Each plot starts with a different target distance and covers half wavelength range. The average distances for Fig. 2(a)–(d) are 0, 1, 2, and 4 m, respectively. Finding the max frequency error for each plot from Fig. 2(a)–(d) and plotting them versus average distances results in Fig. 2(e). The x-axis is the target's average distance in meters, and the y-axis is the max frequency error in hertz. It shows that when the target distance is close to zero, the error from the approximation is negligible. When the target distance is large, the error from the approximation is also large and it becomes nonlinear.

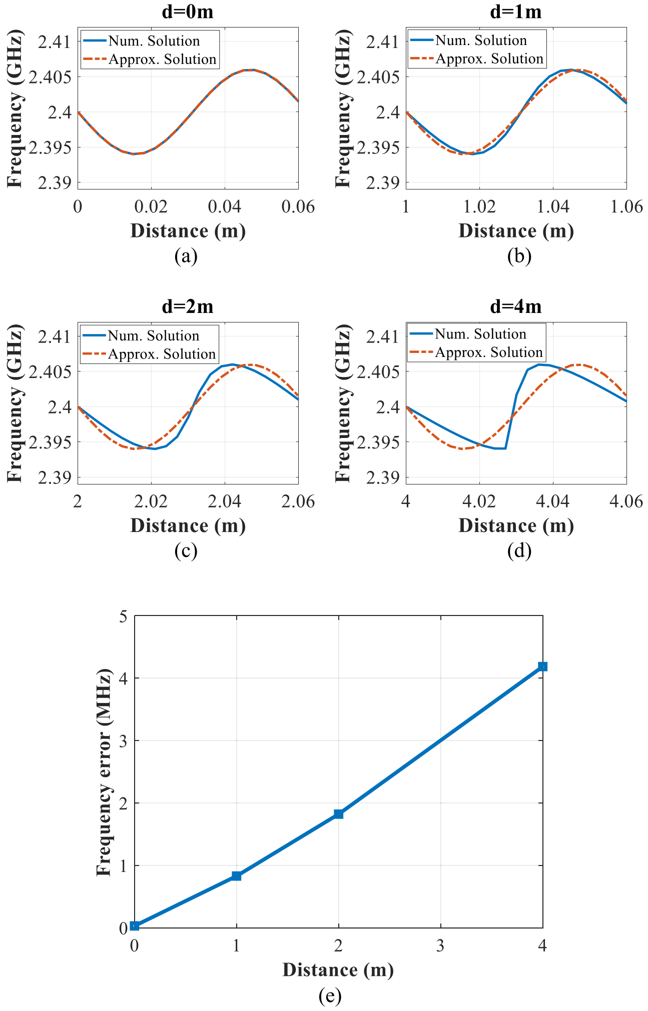

(a) (b) (c) (d) (e)

Fig. 2. Output frequency f_{out} using the approximated (16) versus numerical solution with the original (11). Results for the target distance starting at (a) 0 m, (b) 1 m, (c) 2 m, and (d) 4 m. (e) Maximum frequency error using the approximated equation compared with the numerical solution from the original equation.

Since the instantaneous phase is the time integral of the angular frequency, the oscillator output can be written as

$$T_{\text{SILO}}(t) = \sin\left(\int 2\pi f_{\text{out}} dt\right). \tag{17}$$

Substituting (13) and (16) into (17), the SILO's output can be written as (18), as shown at the bottom of the next page.

Similar to the Doppler radar, the target distance can have a null detection point if $(4\pi d_0/\lambda) = (\pi/2) + k\pi$. However, since this null detection point appears before the down-conversion of the received signals, I/Q quadrature demodulation would not help. The fundamental frequency ω_m is already lost before going to the mixer, as shown in the bottom portion of (18). Assuming the target is at the optimal detection point $(4\pi d_0/\lambda) = k\pi$ for simplicity, the output signal can be calculated as

$$T_{\text{SILO}}(t) \approx \sin\left(2\pi f_0 t \pm \frac{4\pi m}{\lambda} \times \frac{f_L}{f_m} \times \cos(\omega_m t) + C\right) \tag{19}$$

where $f_m = \omega_m/2\pi$, and C is a constant from the integral set by the initial conditions. With a delay-based frequency demodulator [37], T_{SILO} is delayed and mixed with itself. Assume the delay is τ_d, the baseband signal (20), as shown at the bottom of the next page.

As can be seen, the delay τ_d creates a constant phase term, and it introduces another null detection point. This null detection point comes from the static phase difference between the two mixing signals, and I/Q demodulation can help eliminate it. Similarly, $Q(t)$ can be found as

$$Q(t) \approx \frac{1}{2}\sin\left(2\pi f_0 \tau_d \pm \frac{8\pi^2 f_L \tau_d m}{\lambda}\cos(\omega_m t + \varphi)\right). \tag{21}$$

Following the same definition as in the Doppler radar analysis, the modulation gain for the SILO-based radar is defined as $(8\pi^2 f_L \tau_d/\lambda)$.

C. Sensitivity Comparison Between the Conventional Doppler Radar and the SILO-Based Radar

Although the analysis for the SILO-based radar is more complicated than the analysis for the Doppler radar, the final baseband signals' equations are similar. Dividing the SILO-based radar modulation gain by the Doppler radar modulation gain gives the relative modulation gain

$$G_r = 2\pi f_L \tau_d. \tag{22}$$

Substituting (8) into (22)

$$G_r = 2\pi \frac{f_0 |I_{\text{inj}}|}{2Q|I_{\text{osc}}|}\tau_d. \tag{23}$$

Substituting realistic numbers into the equation and evaluating G_r can help understand the sensitivity comparison between Doppler and SILO-based radar. The radar operates at 2.4 GHz. Assuming the oscillator output is 10 dBm, the RX signal or injection signal is −20 dBm, Q is 15, and τ_d is 20 ns, the relative sensitivity strength G_r is calculated to be about 0.316. It means that the SILO-based radar's modulation gain is smaller than the Doppler radar's modulation gain with the assumed parameters. Although SILO-based radar uses frequency modulation and expected to have higher gain, the

---

$$|I(t)| \approx \frac{1}{2}\begin{cases}\left[1 - \left(\frac{4\pi m}{\lambda}\right)^2 \times \frac{1}{2}(1 - \cos(2\omega_m t))\right], & \frac{4\pi d_0}{\lambda} = k\pi \\ \frac{4\pi m \sin(\omega_m t)}{\lambda}, & \frac{4\pi d_0}{\lambda} = \frac{\pi}{2} + k\pi\end{cases} \tag{6}$$

delay-based frequency demodulator it uses has significant attenuation. Despite this, the reason that the SILO-based radar has better sensitivity than the Doppler radar comes from the fact that the SILO-based radar's mixer inputs come from the output of the oscillator directly. In other words, SILO-based radar amplifies the received signal amplitude to be the same level as the oscillator output for free. With the conventional Doppler radar analysis, another 30-dB gain is needed to amplify the −20 dBm received signal to 10 dBm. The relative full path gain can be calculated by including SILO's gain, as shown below

$$G_{r,\text{full}} = 2\pi\frac{f_0\left|I_{\text{inj}}\right|}{2Q\left|I_{\text{osc}}\right|}\tau_d \times \frac{\left|I_{\text{osc}}\right|}{\left|I_{\text{inj}}\right|}\frac{1}{L_d} = 2\pi\frac{f_0\tau_d}{2QL_d} \tag{24}$$

where L_d is the loss of the delay cable. With the same assumption as before, and further assuming $L_d = 1$ dB, $G_{r,\text{full}}$ is evaluated to be about 8.96. Note that the numbers in the assumption are just an example of a typical radar system for vital signs' detection application, and it also assumes that the modulation gain is small such that the small-signal approximation can be applied without considering the Bessel coefficient of the Fourier series [30].

III. PROPOSED SILO-BASED RADAR WITH DUAL NULL DETECTION POINTS' REMOVAL TECHNIQUE

As mentioned in the previous analysis for the SILO-based radar, the target location creates a null detection point that cannot be removed by I/Q quadrature demodulation. To eliminate this null detection point, the proposed circuit needs to be able to affect the phase term in (18). Therefore, a phase shifter is added before the received signal reaches the injection port of the SILO which can serve this purpose. With proper phase shift, it can artificially move the target round-trip phase delay to the optimal distance and off the null detection point. Fig. 3 shows the proposed architecture, where the phase shifter (HMC934LP5E) is added after LNA (HMC476SC70) and before SILO's injection port. The baseband signals $I(t)$ and $Q(t)$ are sent for digital signal processing (DSP). The DSP will determine what is the optimal phase shift. A simple search algorithm can find the optimal setting for the phase shifter by searching for the phase shift with the best signal-to-noise (SNR) ratio. Because the phase shifter is inherently periodic over 360°, there is no need to search in both the directions. In this design, an analog signal-controlled phase shifter is used. The control voltage is swept with 500-mV resolution, which is equivalent to about a 22.5° phase shift. The DSP calculates the FFT for each point and finds the optimal phase shift with the best SNR.

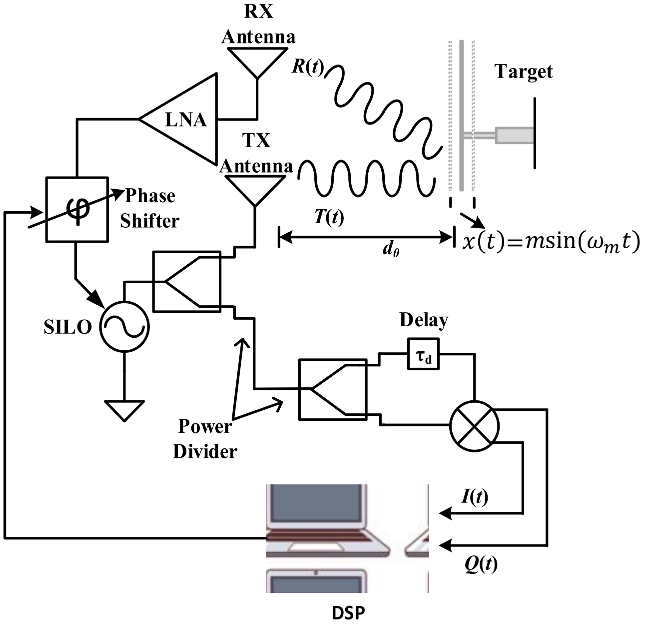

Fig. 3. Block diagram for the proposed SILO radar architecture with dual null point removal.

$$\begin{aligned} T_{\text{SILO}} &= \sin\left(2\pi f_0 t - 2\pi f_L \int \sin\left(\frac{4\pi m\sin(\omega_m t)}{\lambda} + \frac{4\pi d_0}{\lambda}\right)dt\right) \\ &\approx \begin{cases} \sin\left(2\pi f_0 t \pm 2\pi f_L \displaystyle\int \frac{4\pi m \sin(\omega_m t)}{\lambda}dt\right), & \dfrac{4\pi d_0}{\lambda} = k\pi \\ \sin\left(2\pi f_0 t \pm 2\pi f_L \displaystyle\int \left[1 - \left(\frac{4\pi m}{\lambda}\right)^2(1-\cos(2\omega_m t))\right]dt\right), & \dfrac{4\pi d_0}{\lambda} = \dfrac{\pi}{2} + k\pi \end{cases} \end{aligned} \tag{18}$$

$$\begin{aligned} I(t) &= T_{\text{SILO}}(t) \times T_{\text{SILO}}(t-\tau_d) \\ &= \frac{1}{2}\cos\left(2\pi f_0\tau_d \pm \frac{4\pi m}{\lambda} \times \frac{f_L}{f_m} \times (\cos(\omega_m t) - \cos(\omega_m(t-\tau_d)))\right) \\ &= \frac{1}{2}\cos\left(2\pi f_0\tau_d \pm \frac{4\pi m}{\lambda} \times \frac{f_L}{f_m} \times \sqrt{2-2\cos(\omega_m\tau_d)}\cos(\omega_m t + \varphi)\right) \\ &\approx \frac{1}{2}\cos\left(2\pi f_0\tau_d \pm \frac{8\pi^2 m f_L \tau_d}{\lambda}\cos(\omega_m t + \varphi)\right) \end{aligned} \tag{20}$$

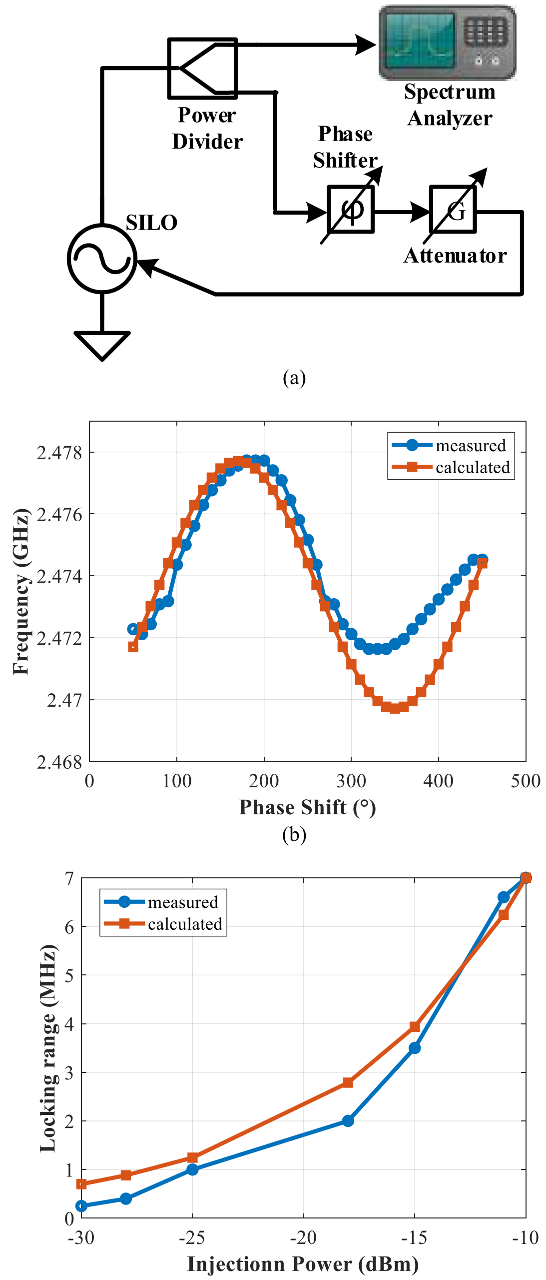

(a)

(b)

(c)

Fig. 4. SILO's characterization experiments. (a) Experiment setup. (b) SILO's output frequency versus phase delay. (c) SILO's locking range versus injection power.

IV. Experimental Results

Several experiments were designed and carried out to validate the proposed theoretical analysis and the performance of the proposed SILO-based radar architecture with dual null detection points' removal.

A. SILO's Frequency Modulation and Locking Range

In the first set of experiments, the SILO's output was connected to a phase shifter (HMC934LP5E) and a programmable attenuator, and then back to the SILO's injection port. The same SILO's output was also sent to a spectrum analyzer with a power divider. The experiment setup is shown in Fig. 4(a). First, for the same attenuation, the phase of the phase shifter was swept, and the frequency from the spectrum analyzer was measured. Fig. 4(b) shows the results. The calculated output frequency from (16) was also plotted on top of the measurement results. As can be seen, both the measurement and calculation results show that the relationship between the output frequency and the phase shift is not linear, and it follows a sinusoidal relationship as predicted.

In the second set of experiments, different attenuations were applied to get different power levels at the injection port of SILO. Then, the phase of the phase shifter was swept for each injection power level to find the maximum and minimum frequencies. The locking range was calculated as half the delta between the maximum and minimum frequencies. Fig. 4(c) shows the locking range of SILO with different injection power levels from the measurement and calculation.

B. Proposed SILO-Based Radar With Dual Null Detection Points' Removal

Although I/Q demodulation is widely used for the SILO-based radar, to the author's knowledge, the reason for doing so is not explained and verified in previous publications [13], [19], [28]. It is worth verifying the I/Q quadrature demodulation in the SILO-based radar addresses the null detection point introduced by the frequency demodulator's delay instead of the null detection point introduced by the target distance. The experiments were set up as shown in Fig. 5(a). An actuator carrying a metal plate (10 cm × 10 cm) was used as the target for better control and repeatable results. A digital phase shifter (HMC647ALP6E) was added to the delay cable in the frequency demodulator to fine-tune the delay, and the baseband outputs $I(t)$ and $Q(t)$ were recorded. Fig. 5(b)–(e) shows the different delay results in different phase relationships for the I and Q channels' outputs. When an additional 140° delay was added, the I channel was at the optimal detection point, and the Q channel was at the null detection point. When an additional 89.6° delay was added, the I and Q channels were in phase. When an additional 33.6° delay was added, the I channel had a null result, while the Q channel had an optimal result. The I and Q channels were out of phase when no phase shift was added. The result shows that the delay in the frequency demodulator indeed creates a null detection point. It also verifies that I/Q quadrature demodulation guarantees that at least one channel's output contains valuable information. When both the I and Q channels are considered, the null detection point from the delay in the frequency demodulator is eliminated.

The next set of experiments was carried out to verify the existence of the other null detection point even with I/Q quadrature demodulation, as well as verify the effectiveness of the proposed architecture on removing the second null detection point. The experiment setup was the same as shown in Fig. 3. The actuator was programmed to oscillate at 1 Hz. The phase shifter's phase was swept, while the baseband transient outputs and their FFTs were recorded. Fig. 6(a) and (b) are the transient output and its FFT output with the target at the

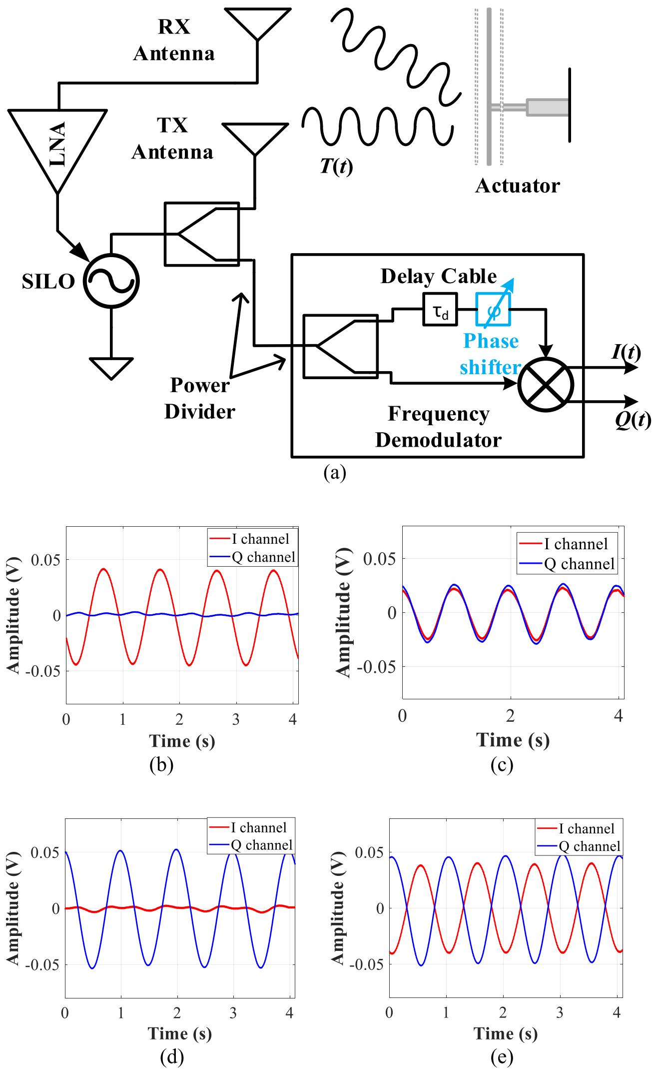

Fig. 5. Experiments for SILO radar's null detection point from delay-based frequency demodulator. (a) Setup of experiments. (b) I/Q signal with a 140° phase delay. (c) I/Q signal with an 89.6° phase. (d) I/Q signal with a 33.6° phase. (e) I/Q signal with a 0° phase.

TABLE I
SENSITIVITY COMPARISON OF DOPPLER AND SILO-BASED RADAR

Configuration	Minimum actuator displacement detected
Doppler radar	1 mm
SILO radar with 2.7m delay cable	0.125 mm
Doppler radar w/o LNA	4 mm
SILO radar with 2.7m delay cable and w/o LNA	1 mm

null detection point. The result shows that the fundamental tone is about −5 dBmV which is below the noise floor near DC. If the target movement was changed to a lower frequency, the tone would have been buried underneath the noise floor. Fig. 6(c) and (d) shows the transient output and its FFT output after sweeping the phase shifter and finding the best phase shift. As can be seen, the signal amplitude increases significantly and stands out from the noise floor. Fig. 6(e) shows the results for the entire sweep. The x-axis is the phase shift in degrees introduced by the phase shifter. The y-axis is the fundamental frequency amplitude in dBmV after applying the FFT. The plot shows that the target amplitude changes with different phase shifts, and the improvement between the optimal phase shift and the null detection point is about 23 dB.

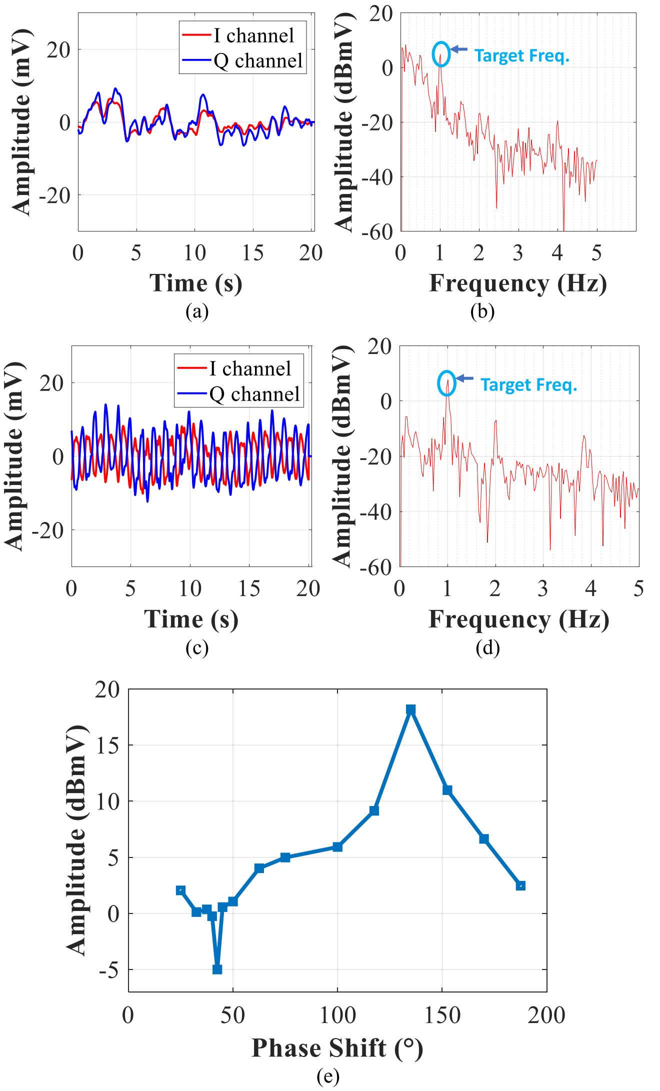

Fig. 6. Experimental results for the proposed dual null detection point removal SILO radar architecture. (a) I/Q channel's transient output for the target at the null detection point. (b) I/Q channels' FFT for the target at the null detection point. (c) I/Q channels' transient output for the target at the optimal detection point. (d) I/Q channels' FFT for the target at the optimal detection point. (e) FFT fundamental tone amplitude versus phase delay from the phase shifter.

C. Comparison of the SILO-Based Radar and the Doppler Radar

Finally, the last set of experiments compared the sensitivity between the SILO-based radar and Doppler radar using the same components. The SILO was reconfigured as the oscillator for the Doppler radar by terminating the injection port with 50 Ω. The SILO's output was then split by a power divider to

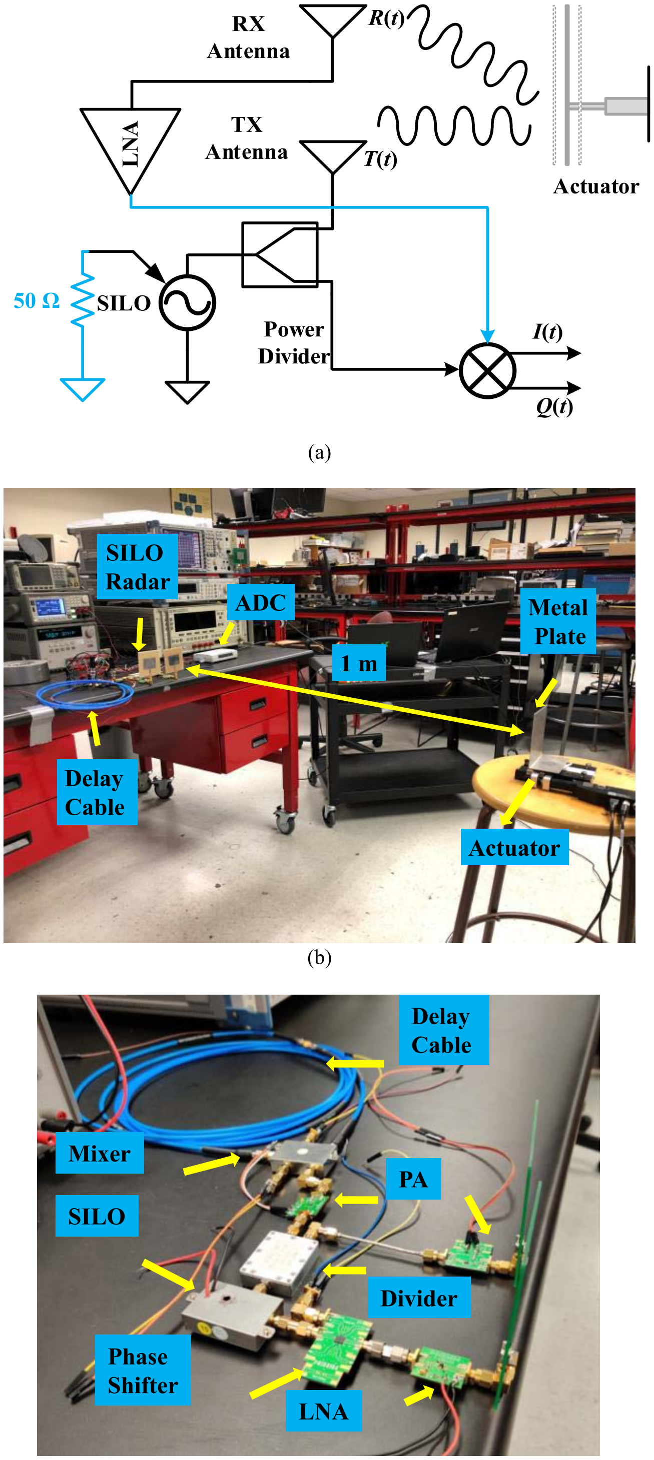

(a)

(b)

(c)

Fig. 7. (a) Block diagram for the Doppler radar experiment setup. (b) In-lab setup of the SILO radar. (c) Close-up photograph of the SILO-based radar.

become the TX signal and LO for the mixer. The delay cable was removed, and the mixer's two inputs were connected to the RX LNA output and LO directly. The system modification is shown in Fig. 7(a). Everything else was the same to ensure a fair comparison. Fig. 7(b) is the in-lab setup of the experiments, and Fig. 7(c) is the close-up photograph of the SILO-based radar. The distance between the actuator and the radar was 1 m, and the frequency of the actuator movement was 1 Hz. A 40-dB baseband amplifier was used, and the data were acquired by a Universal Serial Bus (USB) oscilloscope (Digilent Analog Discovery 2). For each configuration, the actuator displacement amplitude was gradually reduced until the target movement's power was less than 1 dB from the noise floor, and the corresponding displacement of the actuator was recorded as the minimum displacement detected. Table I summarizes the experimental results. To further reduce the power, the experiments were repeated without LNA. The measurement results agree with the expectation that with the same power consumption and components, the SILO-based radar can achieve better sensitivity for the proposed application.

V. CONCLUSION

In this article, a rigorous time-domain analysis for the SILO-based radar with delay-based frequency demodulation is derived and compared with the Doppler radar. It uncovers two null detection points in the SILO-based radar. Furthermore, a solution is proposed for the SILO-based radar to address both null detection points to achieve the best SNR. The I/Q demodulation addresses the null detection point introduced by the delay in the frequency demodulator, and a phase shifter was used to address the null detection point introduced by the target distance. Experiments verified the analysis and demonstrated the effectiveness of the proposed architecture. In the end, the same components were used to build a Doppler radar and an SILO-based radar for an apple-to-apple comparison of sensitivity.

ACKNOWLEDGMENT

The authors would like to thank Dr. F.-K. Wang and Dr. T.-S. Horng with the Department of Electrical Engineering, National Sun Yat-sen University, Kaohsiung, Taiwan, for providing SILO, frequency demodulator, and insightful discussions.

REFERENCES

[1] J. Yan, Z. Peng, H. Hong, H. Chu, X. Zhu, and C. Li, "Vital-SAR-imaging with a drone-based hybrid radar system," *IEEE Trans. Microw. Theory Techn.*, vol. 66, no. 12, pp. 5852–5862, Dec. 2018, doi: 10.1109/TMTT.2018.2874268.

[2] Y. Ma *et al.*, "Non-contact vital states identification of trapped living bodies using ultra-wideband bio-radar," *IEEE Access*, vol. 9, pp. 6550–6559, 2021, doi: 10.1109/ACCESS.2020.3048381.

[3] Y. Ma *et al.*, "Multiscale residual attention network for distinguishing stationary humans and common animals under through-wall condition using ultra-wideband radar," *IEEE Access*, vol. 8, pp. 121572–121583, 2020, doi: 10.1109/ACCESS.2020.3006834.

[4] A. Arbabian, S. Callender, S. Kang, M. Rangwala, and A. M. Niknejad, "A 94 GHz mm-wave-to-baseband pulsed-radar transceiver with applications in imaging and gesture recognition," *IEEE J. Solid-State Circuits*, vol. 48, no. 4, pp. 1055–1071, Apr. 2013, doi: 10.1109/JSSC.2013.2239004.

[5] P. Molchanov, S. Gupta, K. Kim, and K. Pulli, "Short-range FMCW monopulse radar for hand-gesture sensing," in *Proc. IEEE Radar Conf. (RadarCon)*, May 2015, pp. 1491–1496, doi: 10.1109/RADAR.2015.7131232.

[6] H. Sadreazami, M. Bolic, and S. Rajan, "Fall detection using standoff radar-based sensing and deep convolutional neural network," *IEEE Trans. Circuits Syst. II, Exp. Briefs*, vol. 67, no. 1, pp. 197–201, Jan. 2020, doi: 10.1109/TCSII.2019.2904498.

[7] E. Cippitelli, F. Fioranelli, E. Gambi, and S. Spinsante, "Radar and RGB-depth sensors for fall detection: A review," *IEEE Sensors J.*, vol. 17, no. 12, pp. 3585–3604, Jun. 2017, doi: 10.1109/JSEN.2017.2697077.

[8] M. G. Amin, Y. D. Zhang, F. Ahmad, and K. C. D. Ho, "Radar signal processing for elderly fall detection: The future for in-home monitoring," *IEEE Signal Process. Mag.*, vol. 33, no. 2, pp. 71–80, Mar. 2016, doi: 10.1109/MSP.2015.2502784.

[9] W. Ma *et al.*, "A high dynamic range vibration radar sensor with automatic DC voltage extraction," *IEEE Sensors J.*, vol. 22, no. 10, pp. 9945–9955, May 2022, doi: 10.1109/JSEN.2022.3145707.

[10] D. V. Q. Rodrigues, D. Zuo, and C. Li, "Wind-induced displacement analysis for a traffic light structure based on a low-cost Doppler radar array," *IEEE Trans. Instrum. Meas.*, vol. 70, pp. 1–9, 2021, doi: 10.1109/TIM.2021.3098380.

[11] A. C. Amies, C. G. Pretty, G. W. Rodgers, and J. G. Chase, "Experimental validation of a radar-based structural health monitoring system," *IEEE/ASME Trans. Mechatronics*, vol. 24, no. 5, pp. 2064–2072, Oct. 2019, doi: 10.1109/TMECH.2019.2934091.

[12] C. Li *et al.*, "A review on recent progress of portable short-range noncontact microwave radar systems," *IEEE Trans. Microw. Theory Techn.*, vol. 65, no. 5, pp. 1692–1706, May 2017, doi: 10.1109/TMTT.2017.2650911.

[13] F.-K. Wang *et al.*, "Review of self-injection-locked radar systems for noncontact detection of vital signs," *IEEE J. Electromagn., RF Microw. Med. Biol.*, vol. 4, no. 4, pp. 294–307, Dec. 2020, doi: 10.1109/JERM.2020.2994821.

[14] B.-K. Park, O. Boric-Lubecke, and V. M. Lubecke, "Arctangent demodulation with DC offset compensation in quadrature Doppler radar receiver systems," *IEEE Trans. Microw. Theory Techn.*, vol. 55, no. 5, pp. 1073–1079, May 2007, doi: 10.1109/TMTT.2007.895653.

[15] D. Tang, J. Wang, W. Hu, Z. Peng, Y.-C. Chiang, and C. Li, "A DC-coupled high dynamic range biomedical radar sensor with fast-settling analog DC offset cancelation," *IEEE Trans. Instrum. Meas.*, vol. 68, no. 5, pp. 1441–1450, May 2019, doi: 10.1109/TIM.2018.2888917.

[16] D. Tang, J. Wang, Z. Peng, Y.-C. Chiang, and C. Li, "A DC-coupled biomedical radar sensor with analog DC offset calibration circuit," in *Proc. IEEE Int. Instrum. Meas. Technol. Conf. (I2MTC)*, Houston, TX, USA, May 2018, pp. 1–6.

[17] J. Liu, Y. Li, C. Li, C. Gu, and J.-F. Mao, "Accurate measurement of human vital signs with linear FMCW radars under proximity stationary clutters," *IEEE Trans. Biomed. Circuits Syst.*, vol. 15, no. 6, pp. 1393–1404, Dec. 2021, doi: 10.1109/TBCAS.2021.3123830.

[18] J. Tu, T. Hwang, and J. Lin, "Respiration rate measurement under 1-D body motion using single continuous-wave Doppler radar vital sign detection system," *IEEE Trans. Microw. Theory Techn.*, vol. 64, no. 6, pp. 1937–1946, Jun. 2016, doi: 10.1109/TMTT.2016.2560159.

[19] W.-C. Su, P.-H. Juan, D.-M. Chian, T.-S.-J. Horng, C.-K. Wen, and F.-K. Wang, "2-D self-injection-locked Doppler radar for locating multiple people and monitoring their vital signs," *IEEE Trans. Microw. Theory Techn.*, vol. 69, no. 1, pp. 1016–1026, Jan. 2021, doi: 10.1109/TMTT.2020.3037519.

[20] R. E. Arif, W.-C. Su, M.-C. Tang, T.-S. Horng, and F.-K. Wang, "Chest-worn self-injection-locked oscillator tag for monitoring heart rate variability," in *IEEE MTT-S Int. Microw. Symp. Dig.*, Aug. 2020, pp. 512–515, doi: 10.1109/IMS30576.2020.9223983.

[21] G. Paolini, M. Shanawani, D. Masotti, D. M. M.-P. Schreurs, and A. Costanzo, "Respiratory activity monitoring by a wearable 5.8 GHz SILO with energy harvesting capabilities," *IEEE J. Electromagn., RF Microw. Med. Biol.*, vol. 6, no. 2, pp. 246–252, Jun. 2022, doi: 10.1109/JERM.2021.3132201.

[22] F.-K. Wang *et al.*, "A novel vital-sign sensor based on a self-injection-locked oscillator," *IEEE Trans. Microw. Theory Techn.*, vol. 58, no. 12, pp. 4112–4120, Dec. 2010, doi: 10.1109/TMTT.2010.2087349.

[23] M. Ponton and A. Suarez, "Analysis of self-injection locked oscillators for motion sensing applications," in *IEEE MTT-S Int. Microw. Symp. Dig.*, May 2016, pp. 1–4, doi: 10.1109/MWSYM.2016.7538837.

[24] J. Wang, X. Wang, L. Chen, J. Huangfu, C. Li, and L. Ran, "Noncontact distance and amplitude-independent vibration measurement based on an extended DACM algorithm," *IEEE Trans. Instrum. Meas.*, vol. 63, no. 1, pp. 145–153, Jan. 2014, doi: 10.1109/TIM.2013.2277530.

[25] P.-H. Wu, J.-K. Jau, C.-J. Li, T.-S. Horng, and P. Hsu, "Phase- and self-injection-locked radar for detecting vital signs with efficient elimination of DC offsets and null points," *IEEE Trans. Microw. Theory Techn.*, vol. 61, no. 1, pp. 685–695, Jan. 2013, doi: 10.1109/TMTT.2012.2228222.

[26] I. Mostafanezhad and O. Boric-Lubecke, "An RF based analog linear demodulator," *IEEE Microw. Wireless Compon. Lett.*, vol. 21, no. 7, pp. 392–394, Jul. 2011, doi: 10.1109/LMWC.2011.2154318.

[27] D. Girbau, A. M. Roldan, A. Ramos, and R. Villarino, "Remote sensing of vital signs using a Doppler radar and diversity to overcome null detection," *IEEE Sensors J.*, vol. 12, no. 3, pp. 512–518, Mar. 2012, doi: 10.1109/JSEN.2011.2107736.

[28] F.-K. Wang, T.-S. Horng, J.-Y. Shih, Z.-J. Hsu, W.-C. Su, and P.-H. Juan, "See-through-wall (STW) life detector using self-injection-locked (SIL) technology," in *Proc. IEEE Asia–Pacific Microw. Conf. (APMC)*, Dec. 2020, pp. 496–498, doi: 10.1109/APMC47863.2020.9331560.

[29] F.-K. Wang, P.-H. Juan, S.-C. Su, M.-C. Tang, and T.-S. Horng, "Monitoring displacement by a quadrature self-injection-locked radar with measurement- and differential-based offset calibration methods," *IEEE Sensors J.*, vol. 19, no. 5, pp. 1905–1916, Mar. 2019, doi: 10.1109/JSEN.2018.2884729.

[30] C. Li and J. Lin, "Random body movement cancellation in Doppler radar vital sign detection," *IEEE Trans. Microw. Theory Techn.*, vol. 56, no. 12, pp. 3143–3152, Dec. 2008, doi: 10.1109/TMTT.2008.2007139.

[31] R. Adler, "A study of locking phenomena in oscillators," *Proc. IEEE*, vol. 61, no. 10, pp. 1380–1385, Oct. 1973, doi: 10.1109/PROC.1973.9292.

[32] K. Kurokawa, "Injection locking of microwave solid-state oscillators," *Proc. IEEE*, vol. 61, no. 10, pp. 1386–1410, Oct. 1973, doi: 10.1109/PROC.1973.9293.

[33] B. Razavi, "A study of injection locking and pulling in oscillators," *IEEE J. Solid-State Circuits*, vol. 39, no. 9, pp. 1415–1424, Sep. 2004, doi: 10.1109/JSSC.2004.831608.

[34] L. J. Paciorek, "Injection locking of oscillators," *Proc. IEEE*, vol. 53, no. 11, pp. 1723–1727, Nov. 1965.

[35] H. L. Stover, "Theoretical explanation for the output spectra of unlocked driven oscillators," *Proc. IEEE*, vol. 54, no. 2, pp. 310–311, Feb. 1966.

[36] M. Armand, "On the output spectrum of unlocked driven oscillators," *Proc. IEEE*, vol. 57, no. 5, pp. 798–799, May 1969.

[37] H. Gheidi and A. Banai, "An ultra-broadband direct demodulator for microwave FM receivers," *IEEE Trans. Microw. Theory Techn.*, vol. 59, no. 8, pp. 2131–2139, Aug. 2011, doi: 10.1109/TMTT.2011.2144993.

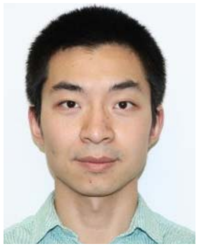

Dongyang Tang (Student Member, IEEE) received the B.Sc. degree in microelectronics from Sichuan University, Chengdu, China, in 2011, the M.Sc. degree in electrical engineering from the University of Michigan, Ann Arbor, MI, USA, in 2013, and the Ph.D. degree in electrical engineering from Texas Tech University, Lubbock, TX, USA, in 2022.

He joined Qualcomm, San Diego, CA, USA, in 2013, as a Mixed-Signal IC Design Engineer. He is currently a Staff Engineer with the Qualcomm MSIC Group, San Diego. His research interests include mixed-signal integrated circuits and systems and RF integrated circuits and systems.

Davi V. Q. Rodrigues (Graduate Student Member, IEEE) received the B.S. degree in communications engineering from the Military Institute of Engineering, Rio de Janeiro, Brazil, in 2017. He is currently pursuing the Ph.D. degree in electrical engineering at Texas Tech University, Lubbock, TX, USA.

From 2009 to 2011, he was with the Brazilian Navy. He became a member of the Brazilian Army in 2013. He was commissioned as a First Lieutenant of the Military Engineers Branch in 2017. In the spring/summer of 2018, he served for the Southern Military Command, Porto Alegre, Rio Grande do Sul, Brazil. He joined Texas Tech University as a Research Assistant in the fall of 2018. In the summer of 2021, he was with Uhnder, Inc., Austin, TX, USA, where he was involved in the design and evaluation of signal processing algorithms for the mitigation of radar interference. In the spring/summer of 2022, he was with Abbott Laboratories, Los Angeles, CA, USA, where he was involved in the design of antennas and microwave systems for next-generation implantable medical devices. His research interests include structural health monitoring based on Doppler radars, wireless sensors for smart living and biomedical applications, and microwave/millimeter-wave circuits and systems.

Mr. Rodrigues was a recipient of the Best Student Paper Award of the 2020 IEEE MTT-S International Microwave Biomedical Conference (IMBioC), the Best Paper Award—Antennas Category of the 2020 IEEE MTT-S Asia–Pacific Microwave Conference (APMC), and the Best Student Paper Award—Honorable Mention of the 2021 IEEE MTT-S International Wireless Symposium (IWS). He was a Finalist of the Student Paper Contest at the 2021 IEEE MTT-S Radio Wireless Week (RWW). He also received the First Prize Award of the IEEE MTT-S International Microwave Symposium (IMS) Adaptive Relay Transceiver Design Competition in 2019, the Second Prize Award of the IEEE MTT-S IMS High-Sensitivity Motion Radar Design Competition in 2019 and 2021, and the IEEE MTT-S Graduate Fellowship Award and the prestigious IEEE MTT-S Tom Brazil Graduate Fellowship Award in 2022.

Michael C. Brown (Graduate Student Member, IEEE) received the B.S. and M.S. degrees in electrical engineering from Texas Tech University, Lubbock, TX, USA, in 2017 and 2019, respectively, where he is currently pursuing the Ph.D. degree in electrical engineering.

From summer 2019 to fall 2020, he was an Intern with the Los Alamos National Laboratory, Los Alamos, NM, USA, where he was involved in various radar signal processing and modeling projects. His research interests include passive microwave structures, radar signal processing, and phase modulated radar design and applications.

Mr. Brown was a recipient of the NXP Graduate Fellowship in 2021.

Changzhi Li (Senior Member, IEEE) received the B.S. degree in electrical engineering from Zhejiang University, Hangzhou, China, in 2004, and the Ph.D. degree in electrical engineering from the University of Florida, Gainesville, FL, USA, in 2009.

He is currently a Professor with Texas Tech University, Lubbock, TX, USA. His research interests include microwave/millimeter-wave sensing for healthcare, security, energy efficiency, structural monitoring, and human–machine interface.

Dr. Li is the IEEE Microwave Theory and Techniques Society (MTT-S) Distinguished Microwave Lecturer, Tatsuo Itoh class of 2022–2024. He was a recipient of the IEEE MTT-S Outstanding Young Engineer Award, the IEEE Sensors Council Early Career Technical Achievement Award, the American Society of Engineering Education (ASEE) Frederick Emmons Terman Award, the IEEE-Eta Kappa Nu (HKN) Outstanding Young Professional Award, the NSF Faculty Early CAREER Award, and the IEEE MTT-S Graduate Fellowship Award. He is an Associate Editor of the IEEE TRANSACTIONS ON MICROWAVE THEORY AND TECHNIQUES and the IEEE JOURNAL OF ELECTROMAGNETICS, RF AND MICROWAVES IN MEDICINE AND BIOLOGY.